Core−shell Nanostructured Nanopowders along $(CeO_x)_x(Al_2O_3)_{1-x}$ Tie-Line by Liquid-Feed Flame Spray Pyrolysis (LF-FSP)

Min Kim, Thomas R. Hinklin, and Richard M. Laine*

Department of Materials Science and Engineering, University of Michigan, Ann Arbor, Michigan 48109-2136

Received November 28, 2007. Revised Manuscript Received May 18, 2008

We report here the synthesis of $(CeO_x)_{1-x}(Al_2O_3)_x$ mixed-metal oxide nanopowders with molar ratios that span the $CeO_x-Al_2O_3$ composition range. Liquid-feed flame spray pyrolysis (LF-FSP) of mixtures of $N(CH_2CH_2O)_3Al$ (alumatrane) and $Ce(O_2CCH_2CH_3)(OH)$ precursors dissolved in ethanol were aerosolized with O_2, combusted at temperatures of 1500−2000 °C and rapidly quenched thereafter to provide $(CeO_x)_{1-x}(Al_2O_3)_x$ nanopowders of selected compositions. All powders exhibit average particle sizes (APSs) < 20 nm and corresponding surface areas of ≥50 m^2/g when produced at rates of 100−300 g/h. The as-processed powders were characterized in terms of phase, size, specific surface area, composition, and morphology by BET, XRD, XRF, SEM, TEM, STEM, XEDS, XPS, FT-IR, and TGA-DTA. Surprising core−shell nanostructured nanopowders are observed in the Ce−Al−O system at CeO_x rich concentrations (≥15 mol %). In addition, evidence is presented for the incorporation of Ce^{3+} ions in the δ-alumina lattice at the lowest concentrations and Ce-magnetoplumbite ($CeAl_{11}O_{18}$) at 5−10 mol % CeO_x concentrations.

Introduction

Ceria-based mixed-metal oxides are important candidates for a wide range of applications. Besides well-known catalytic applications related to the reversible Ce^{4+}/Ce^{3+} redox couple,[1–3] mixed-metal oxides with ceria are currently receiving attention as phosphors,[4–6] chemical mechanical polishing (CMP) slurries,[7,8] cutting tools (ceria-toughened alumina),[9] and oxygen transport media for solid oxide fuel cells (SOFC).[10–12]

The ceria−alumina mixed-metal oxide system is of particular interest for catalytic applications, because rare earth (RE) species have the potential to stabilize high-surface-area transition aluminas.[13] These materials have been a topic of significant research[14,15] because the gradual sintering and transformation of γ-Al_2O_3 into α-Al_2O_3 above 1000 °C coarsens the alumina substrate, leading to loss of catalytic activity due to the reduction of the accessible surface area of the catalyst and changes in the acid/base surface chemistry.

For ceria−alumina binary systems, highly dispersed Ce^{3+} ions form $CeAl_{11}O_{18}$ and $CeAlO_3$ by solid-state interaction between Al_2O_3 and CeO_x at ≥5 mol% ceria compositions.[16,17,39,40] In this case, Ce^{3+} ions replace Al^{3+} in the transition alumina lattice increasing the thermal stability of δ-alumina by forming metastable Ce-magnetoplumbite ($CeAl_{11}O_{18}$) thereby halting Al_2O_3 grain growth.[39,40] It has been reported that the addition of rare earth (RE) ions to transition alumina-supported Pd catalysts not only reduces sintering of the alumina support at higher temperatures (around 1000 °C), but also retards sintering of the supported Pd.[16–18]

While stabilization of surface area is a classical field of study for rare-earth-doped transition aluminas, our interest in these materials centers on their emissive behavior for potential use as laser paints and for other photonic applications.[19–21] Thus, we recently reported lasing behavior from RE-doped mixed-metal oxide nanocomposites under cathodoluminescence conditions.[20,21] In related systems, we demonstrated that RE-doped mixed-metal oxide nanopowders

* Corresponding author. E-mail: talsdad@umich.edu.

(1) Jen, H. W.; Graham, G. W.; Chun, W.; McCabe, R. W.; Cuif, J. P.; Deutsch, S.; Touret, O. *Cat. Today* **1999**, *50*, 309.
(2) Marecot, P.; Pirault, L.; Mabilon, G.; Prigent, M.; Barbier, J. *Appl. Catal., B* **1994**, *5*, 57.
(3) McCabe, R. W.; Kisenyi, J. M. *Chem. Ind.* **1995**, *15*, 605.
(4) Zhang, K.; Liu, H.; Wu, Y.; Hu, W. *J. Mater. Sci.* **2007**, *42*, 9200.
(5) Kalivas, N.; Valais, I.; Nikolopoulos, D.; Konstantinidis, A.; Gaitanis, A.; Cavouras, D.; Nomicos, C. D.; Panayiotakis, G.; Kandarakis, I. *Appl. Phys. A* **2007**, *89*, 443.
(6) Milosevic, O.; Mancic, L.; Rabanal, M. E.; Torralba, J. M.; Yang, B.; Townsend, P. *J. Electrochem. Soc.* **2005**, *152* (9), G707.
(7) Hedge, S.; Babu, S. V. *Electrochemical Solid-State Lett.* **2004**, *7* (12), G316.
(8) Lim, G.; Lee, J.; Kim, J.; Lee, H.; Hyun, S. *Mater. Sci. Forum* **2004**, *449−452*, 1105.
(9) Kumar, A. S.; Durai, A. R.; Sornakumar, T. *Powder Metall.* **2004**, *47* (3), 235.
(10) Huang, B.; Ye, X. F.; Wang, S. R.; Nie, H. W.; Liu, R. Z.; Wen, T. L. *Mater. Res. Bull.* **2007**, *42*, 1705.
(11) Laosiripojana, N.; Assabumrungrat, S. *Appl. Catal., A* **2007**, *320*, 105.
(12) Soorie, M.; Skinner, S. J. *Solid State Ionics* **2006**, *177*, 2081.
(13) Piras, A.; Trovarelli, A.; Dolcetti, G. *Appl. Catal. B* **2000**, *28*, L77.
(14) Ahlstrom-Silversand, A. F.; Odenbrand, C. U. I. *Appl. Catal.* **1997**, *153*, 157.
(15) Arai, H.; Machida, M. *Appl. Catal. A* **1996**, *138* (2), 161.
(16) Church, J. S.; Cant, N. W.; Trimm, D. L. *Appl. Catal. A.* **1993**, *101*, 105.
(17) Pettigrew, D. J.; Trimm, D. L.; Cant, N. W. *Catal. Lett.* **1994**, *28*, 313.
(18) Chang, J.; Chou, T. *Appl. Catal. A.* **1997**, *156*, 193.
(19) (a) Laine, R. M.; Rand, S. C.; Hinklin, T. R.; Williams, G. R. U.S. Patent 6,656,588 **2003**. (b) Hinklin, T. R.; Ph.D. dissertation,2006, University of Michigan.
(20) Li, B.; Williams, G. R.; Rand, S. C.; Hinklin, T. R.; Laine, R. M. *Opt. Lett.* **2002**, *27* (6), 394.
(21) Williams, G. R.; Bayram, S. B.; Rand, S. C.; Hinklin, T. R.; Laine, R. M. *Phys. Rev. A* **2001**, *65*, 013807.

10.1021/cm703382x CCC: $40.75
Published on Web 07/24/2008

offer novel UV emission behavior.[20,21] This research is potentially relevant to improving phosphors for field emission displays, X-ray imaging, nanocomposite lasers, and other photonic applications.[22–24]

All nanopowders used in these previous studies were synthesized using LF-FSP, which offers the potential to make a wide variety of single and mixed-metal oxide nanopowders in a single step.[25–32] The LF-FSP process aerosolizes metalloorganic precursors dissolved in an alcohol solvent with oxygen, combusts the aerosol within a quartz chamber at ≥1500 °C, and then rapidly quenches the gaseous species to produce nanosize oxide "soot" with the same compositions as those in the starting precursor solutions. See the experimental section below for details.

To date, we have used LF-FSP to make phase-pure nanopowders of single and mixed-metal oxides including Al_2O_3, CeO_2, ZrO_2, TiO_2, CoO and NiO.[26–32] These LF-FSP as-produced nanopowders are typically unaggregated with specific surface areas (SSAs) of 30−50 m^2/g and average particle sizes (APSs) of 15−30 nm.

We have focused on oxide systems that offer potential for catalytic and/or photonic applications.[29–32] According to these studies, LF-FSP is proven to be a low-cost, single-step route to versatile materials in mixed-metal oxide systems and provides easy access to many types of metal oxide nanopowders with excellent control of phase purity and morphology. These nanopowders in turn offer potential access to a wide variety of dense ceramic source materials for catalytic, mechanical, photonic, electrical, and electronic applications.

Here we use LF-FSP to explore the synthesis and properties of nanopowders along the $(CeO_x)_x(Al_2O_3)_{1-x}$ tieline. Unlike previous studies on ceria-alumina mixed-metal oxides materials,[1–12] we find new nanostructured nanopowders for each composition. As with other LF-FSP products, the resulting unaggregated nanopowders offer specific surface areas (SSAs) ≥ 50 m^2/g and average particle sizes (APSs) less than 20 nm without microporosity.

Surprisingly, LF-FSP with the correct choice of metal-loorganic precursors provides access to core−shell nanopowders in a single step for certain composition of $(CeO_x)_x$-$(Al_2O_3)_{1-x}$.

Experimental Section

Liquid-Feed Flame Spray Pyrolysis (LF-FSP). LF-FSP, as invented at the University of Michigan, has been described in detail in published papers.[25–32] Briefly, alcohol (typically EtOH) solutions containing 1−10 wt % loading of ceramic as precursors, e.g., single- or mixed-metal alkoxides, carboxylates, or β-diketonates, are aerosolized at ∼100 mL/min with O_2 into a 1.5 m long quartz chamber, where they are ignited with methane pilot torches.

Initial combustion temperatures run 1500−2000 °C, depending on the processing conditions, generating nanopowder "soot." Temperatures drop to 300−500 °C over 1.5 m, equivalent to a 1000 °C quench in ≤100 ms leading to kinetic nanopowders that are carried away from the combustion area by the natural flow of gases aided by a high-velocity (>700 cfm) inline blower. Resulting nanopowders are largely unaggregated, although they are lightly agglomerated.

Yield can be 200 g/h when using wire-in-tube electrostatic precipitators operating at 10 kV. Typical powders are 15−100 nm APS with specific surface areas (SSAs) of 30−100 m^2/g. When combinations of elements are used, the resulting nanopowders will have compositions identical to those of the precursor solutions. Because compositions of chemical solutions can be changed intentionally, potentially even during mixing just before aerosolization, it becomes possible to combinatorially produce mixed-metal oxide materials. Hence it becomes possible to rapidly optimize materials for given properties or for ease of processing.

Caution! *Note that combustion of large quantities of precursor in ethanol in an oxygen atmosphere can be extremely hazardous. Good exhaust systems and a detailed standard operating procedure should be developed prior to attempting these types of experiments.*

Materials. *Alumatrane.* $N(CH_2CH_2O)_3Al$ prepared as described previously[33,34] is used as the alumina source.

Cerium Propionate. Cerium carbonate [$Ce_2(CO_3)_3 \cdot x(H_2O)$, 99%, 70 g, 0.15 mol] was reacted with excess propionic acid (400 mL, 5.44 mol) in a 1 L flask equipped with a still head and an addition funnel. N_2 was sparged directly through the solution (2 psi pressure) as the solution was heated at 120 °C for 2 h to distill off ∼150 mL of liquid (water and propionic acid). The ceramic loading of the resulting precursor was 9 wt % as determined by TGA.

XRD Studies. As-prepared samples were characterized using a Rigaku rotating anode goniometer. Powder samples were prepared by placing ∼100 mg on XRD sample holders (amorphous silica slides) for data collection. Cu Kα (λ = 1.54 Å) radiation with a Ni filter was used with a working voltage and current of 40 kV and 100 mA, respectively. Scans were continuous from 10−80° 2θ with a step scan of 2° 2θ/min in increments of 0.05° 2θ. Peak positions and relative intensities were characterized by comparison with PDF files of standard materials: CeO_2 (PDF file 4−002−2713), δ*-Al_2O_3 (PDF file 46−1215), $CeAl_{11}O_{18}$ (PDF file 00−048−0055). Debye−Scherrer line broadening was used to calculate average particle sizes (APS) from the XRD powder patterns.

X-ray Fluorescence (XRF). Chemical analyses were obtained by X-ray fluorescence (XRF) from Ford motor company (Dearborn, MI). Samples were prepared by mixing 0.50 g of sample into 10.0 g of $Li_2B_4O_7$ glass flux. The sample and glass flux were mechanically stirred for 5 min in a methacrylate vial with three methacrylate balls using a SPEX 6000 ball mill. The mixtures were fused into glass beads by placing them in an oven held at 1000 °C for 10 min. The samples were analyzed using a Panalytical PW2400 X-Ray fluorescence spectrometer (formerly Philips), equipped with a WDS detection system (wavelength dispersive).

(22) Chiang, C.; Tsai, M.; Hon, M. *J. Electrochem. Soc.* **2007**, *154* (10), J326.
(23) Touš, J.; Blaz[GRAPHIC]ek, K.; Pína, L.; Sopko, B. *Radia. Meas.* **2007**, *42*, 925.
(24) Yuan, J.; Wang, J.; Xiong, D.; Zhao, J.; Fu, Y.; Zhang, G.; Shi, C. *J. Lumin.* **2007**, *126*, 717.
(25) Marchal, J.; Johns, T.; Baranwal, R.; Hinklin, T.; Laine, R. M. *Chem. Mater.* **2004**, *16*, 822.
(26) Bickmore, C. R.; Waldner, K. F.; Baranwal, R.; Hinklin, T.; Treadwell, D. R.; Laine, R. M. *J. Europ. Ceram. Soc.* **1998**, *18*, 287.
(27) Laine, R. M.; Hinklin, T. R.; Williams, G. R.; Rand, S. C. *Mat. Sci. Forum* **2000**, *343-346*, 500.
(28) Hinklin, T.; Toury, B.; Gervais, C.; Babonneau, F.; Gislason, J. J.; Morton, R. W.; Laine, R. M. *Chem. Mater.* **2004**, *16*, 21.
(29) Kim, S.; Gislason, J. J.; Morton, R. W.; Pan, X. Q.; Sun, H. P.; Laine, R. M. *Chem. Mater.* **2004**, *16*, 2336.
(30) Azurdia, J. A.; Marchal, J.; Shea, P.; Sun, H.; Pan, X. Q.; Laine, R. M. *Chem. Mater.* **2006**, *18*, 731.
(31) Azurdia, J. A.; Marchal, J.; Laine, R. M. *J. Am. Ceram. Soc.* **2006**, *89* (9), 2749.
(32) Kim, M.; Laine, R. M. *J. Cer. Proc. Res.* **2007**, *8*, 129.
(33) Hinklin, T.; Mueller, B. L.; Laine, R. M. U.S. Patent 5,418,298, 1995.
(34) Narayanan, R.; Laine, R. M. *App. Org. Chem.* **1997**, *11*, 919.

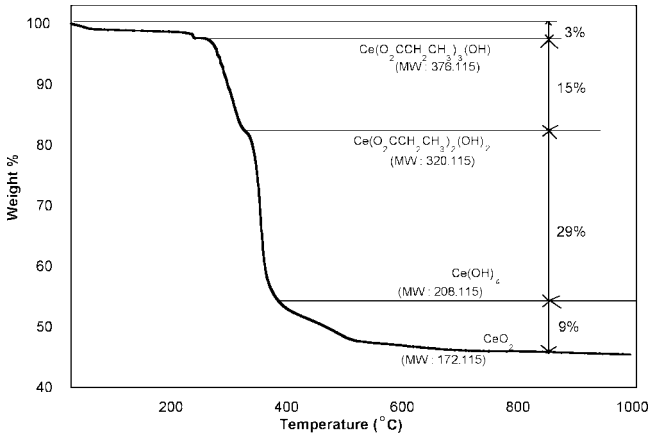

Figure 1. TGA of $Ce(O_2CCH_2CH_3)_3(OH)$ ramped at 10 °C/min in synthetic air.

X-Ray Photoelectron Spectroscopy (XPS). Kratos Axis Ultra XPS (Kratos analytical, Manchester, U.K.) were used to identify chemical elements and their oxidation state, especially for cerium ions in our nanopowders. Powder samples were prepared by placing 0.50 g of nanopowders in a high vacuum chamber ($\sim 1 \times 10^{-9}$ torr). Monochromatic Al Kα ($\lambda = 9.89$ Å) were used as X-ray source to measure binding energy of chemical elements. After 2 min of one survey scan, 20 times of specific element scan (for cerium ions) were performed and average resulting peaks are presented. Quantification of resulting peaks was performed by the CasaXPS program.

Thermal Gravimetric Analysis and Differential Thermal Analysis (TGA/DTA). TGA-DTA were performed using a SDT 2960 Simultaneous Differential Thermal Analyzer (TA Instruments, Inc., New Castle, DE). The instrument was calibrated with gold supplied by Perkin-Elmer. Samples (70 mg) of as-prepared powders were hand pressed in a 3 mm dual action die and placed inside Pt sample cups and heated at ramp rates of 10 °C/min from ambient temperature to 1400 °C. The reference material was a pellet of α-alumina. A flow of synthetic air, 50 mL/min, was maintained during all experiments.

Specific Surface Area (SSA). SSA was measured on a Micromeritics ASAP 2000 sorption analyzer. Samples (200 mg) were degassed at 400 °C until the outgas rate was 5 Torr/min. Analyses was run at 77 K with N_2. SSAs were determined by the BET multipoint method using at least five data points with relative pressures of 0.001−0.20. The average particle size was derived using the formula $\langle R \rangle = 6/(\rho \times SSA)$ where $\langle R \rangle$ is the average particle size in diameter and ρ is the density of the material. The densities of the mixed powders were calculated using the rule of mixtures, which is an accepted method of obtaining the values for the properties of well-behaved composite materials, such as these intimately mixed nanopowders. The rule of mixtures is a weighted average using the volumetric fraction of the phases present rather than the mass fraction.

Rule of Mixtures: $P_c = P_a v_a + P_b v_b$, where P is a property and v is volume fraction.

Scanning Electron Microscopy (SEM). A high-resolution SEM (FEI NOVA Dual beam focused ion beam workstation and scanning electron microscope) was used to image powder morphologies. Powder samples were dispersed in distilled H_2O using an ultrasonic horn (Vibra-cell, Sonics and Materials, Inc., Newton, CT). A drop of the dispersed powder/water was placed on an aluminum SEM stub and allowed to dry for 4 h on a hot plate. Powders were sputter coated with 1−5 nm of Au−Pd to reduce charging effects. The operating voltage was 15.0 kV.

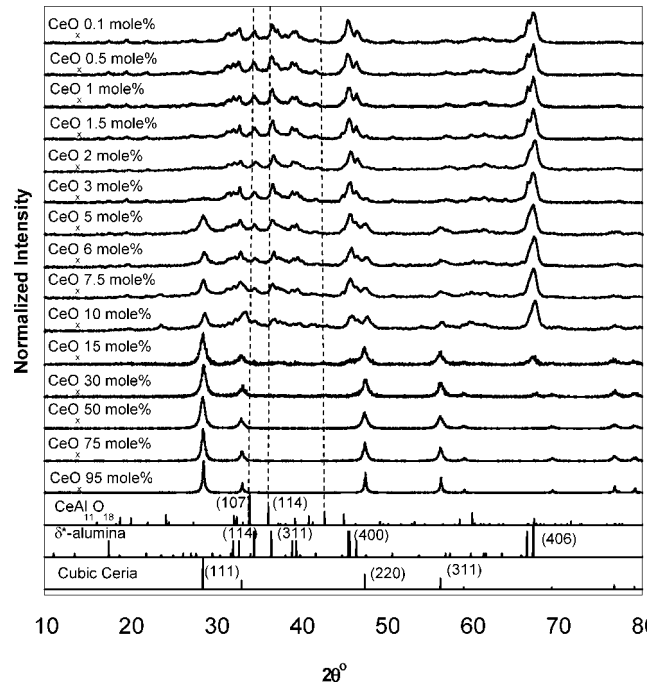

Figure 2. XRD powder patterns of as-produced $(CeO_x)_x(Al_2O_3)_{1-x}$ nanopowders by LF-FSP. Dashed lines show major magnetoplumbite diffraction peaks. CeO_x (PDF file 4−002−2713), δ^*-Al_2O_3 (PDF file 46−1215), $CeAl_{11}O_{18}$ (PDF file 00−048−0055).

Table 1. APSs and SSAs of $(CeO_2)_x(Al_2O_3)_{1-x}$ Nanopowders

sample mole % ceria	XRD line broadening particle size (nm)	BET-derived particle size (nm)	SSA (m^2/g)
95	20 ± 1	20 ± 1	45
75	18 ± 1	20 ± 1	45
50	16 ± 1	20 ± 1	50
30	15 ± 1	20 ± 1	57
15	15 ± 1	20 ± 1	60
10	14 ± 1	22 ± 1	57
7.5	17 ± 1	22 ± 1	63
6	15 ± 1	24 ± 1	61
5	14 ± 1	24 ± 1	60
3	14 ± 1	26 ± 1	56
2	14 ± 1	26 ± 1	58
1.5	16 ± 1	24 ± 1	62
1	15 ± 1	22 ± 1	65
0.5	14 ± 1	20 ± 1	70
0.1	12 ± 1	22 ± 1	66

Transmission Electron Microscopy (TEM). An analytical high resolutionx TEM (model 3011, JEOL, Osaka, Japan) was used to measure the particle sizes and morphologies of as-prepared powders. Powder samples were prepared by dipping a holey carbon grid in a vial of emulsion with as-prepared powder. The specimen was held in a Gatan double tilt goniometer. An operating voltage of 300 kV was used.

Scanning Transmission Electron Microscopy (STEM)/X-ray Energy Dispersive Spectroscopy (XEDS). An analytical STEM (model 2010, JEOL, Osaka, Japan) with X-ray energy dispersive spectroscopy (XEDS) was used to determine core and shell elements of nanosized particles. The same samples from high-resolution TEM were used. The operating voltage was 200 kV.

FTIR Spectra. Diffuse reflectance Fourier transform (DRIFT) spectra were recorded on a Thermo Fisher Scientific Nicolet 6700 FTIR spectrometer (Thermo Fisher Scientific, Inc., Madison, WI). Optical grade, random cuttings of KBr (International Crystal Laboratories, Garfield, NJ) were ground, with 1.0 wt % of the sample to be analyzed. For DRIFT analysis, samples were packed firmly and leveled off at the upper edge to provide a smooth surface.

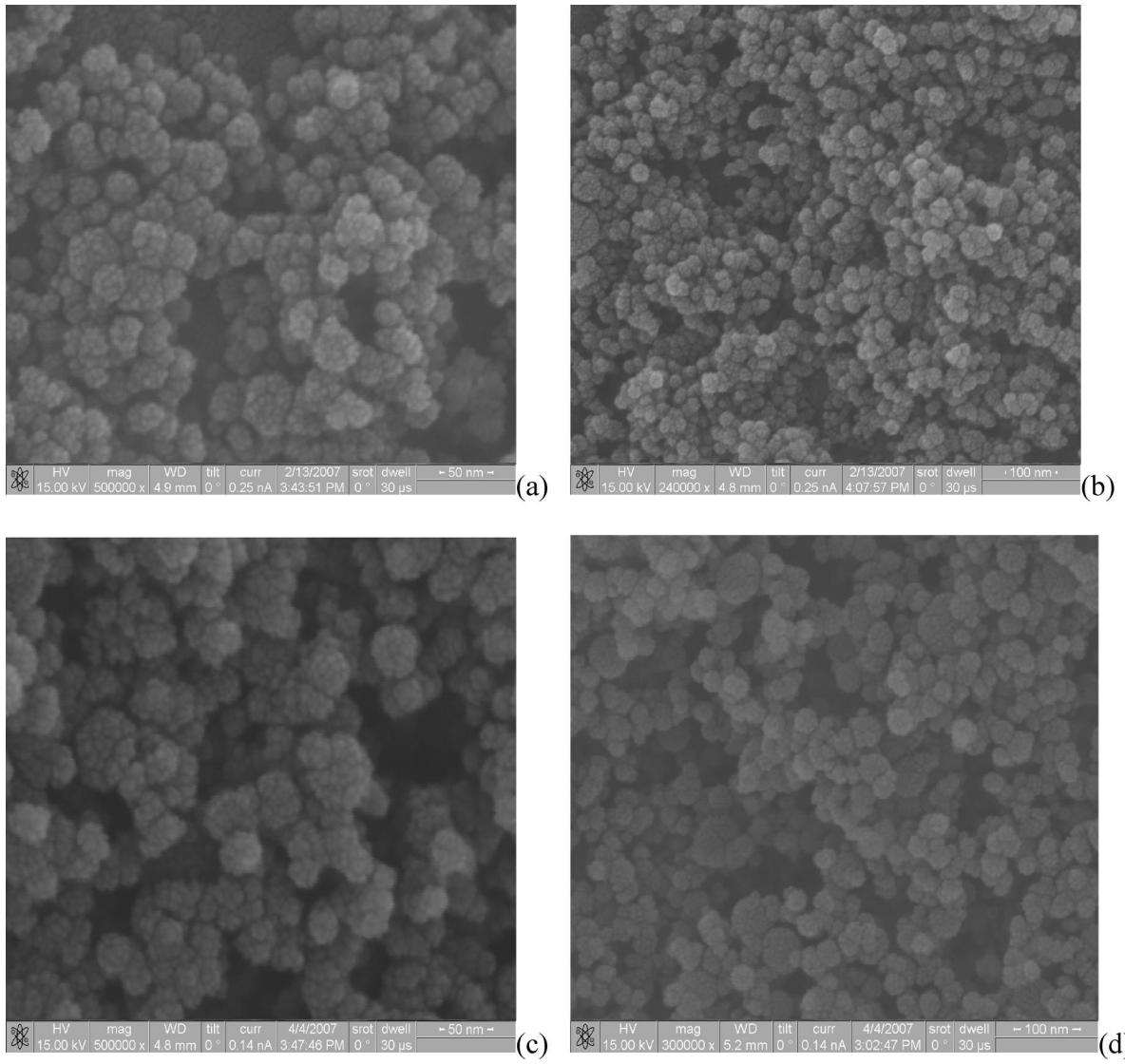

Figure 3. SEM images of (a) 75 mol % CeO_x in Al_2O_3, (b) 50 mol % CeO_x in Al_2O_3, (c) 10 mol % CeO_x in Al_2O_3, and (d) 0.5 mol % CeO_x in Al_2O_3.

For transmission IR, 100 mg of each sample prepared for DRIFT analysis was pressed in a stainless steel double action die (12.75 mm diameter) at 100 MPa for 1 min in a Carver Press (model 3912). Fresh backgrounds of pure KBr were done every hour. The FTIR sample chamber was flushed continuously with N_2 prior to data acquisition in the range 4000−400 cm^{-1}. Each run consisted of 128 scans with a resolution of ±4 cm^{-1}.

Results and Discussion

The objectives of the current studies are to produce and characterize high surface area, nonporous nanopowders along the $(CeO_x)_x(Al_2O_3)_{1-x}$ tie-line in one step using LF-FSP as a prelude to exploring their potential utility for catalytic,[1–3] photonic,[4–6] and structural applications.[7–9]

Nanopowders prepared along the $(CeO_x)_x(Al_2O_3)_{1-x}$ tie-line differ from other conventionally prepared nanomaterials as noted above, because LF-FSP provides single step access to core−shell nanopowders. Current methods of making coated nanoparticles are mostly based on solution phase methods, and primarily sol−gel processing.[35–38] These types of methods are usually multi-step.[35–38] They usually require homogeneous dispersions of core materials in a solvent, typically by ultrasonication, followed by coating with the shell materials. The latter step often leads to micrometer-sized final products and aggregation of the core powders is unavoidable unless processing is done at low concentrations. Also, these multistep processes are inefficient in time, cost and homogeneity of final product.[35–38] In contrast, LF-FSP has the potential to provide simple and efficient routes to nano core−shell nanopowders without aggregation.

In the following section, we begin by characterizing the ceria precursor developed for LF-FSP processing. Thereafter we follow with sections on the production of selected

(35) Jia, Y.; Hotta, Y.; Sato, K.; Watari, K. *J. Am. Ceram. Soc.* **2006**, *89* (3), 1103.
(36) Chang, S.; Liu, L.; Asher, S. *J. Am. Chem. Soc.* **1994**, *116*, 6739.
(37) Ruys, A. J.; Mai, Y. *Mater. Sci. Eng.* **1999**, *A265*, 202.
(38) Ferguson, J. D.; Buechler, K. J.; Weimer, A. W.; George, S. M. *Powder Technology* **2005**, *156*, 154.
(39) Iyi, N.; Takekawa, S.; Kimura, S. *J. Solid State Chem.* **1989**, *83*, 8.
(40) Jansen, S. R.; De haan, J. W.; Van de ven, L. J. M.; Hanssen, R.; Hintzen, H. T.; Metselaar, R. *Chem. Mater.* **1997**, *9*, 1516.

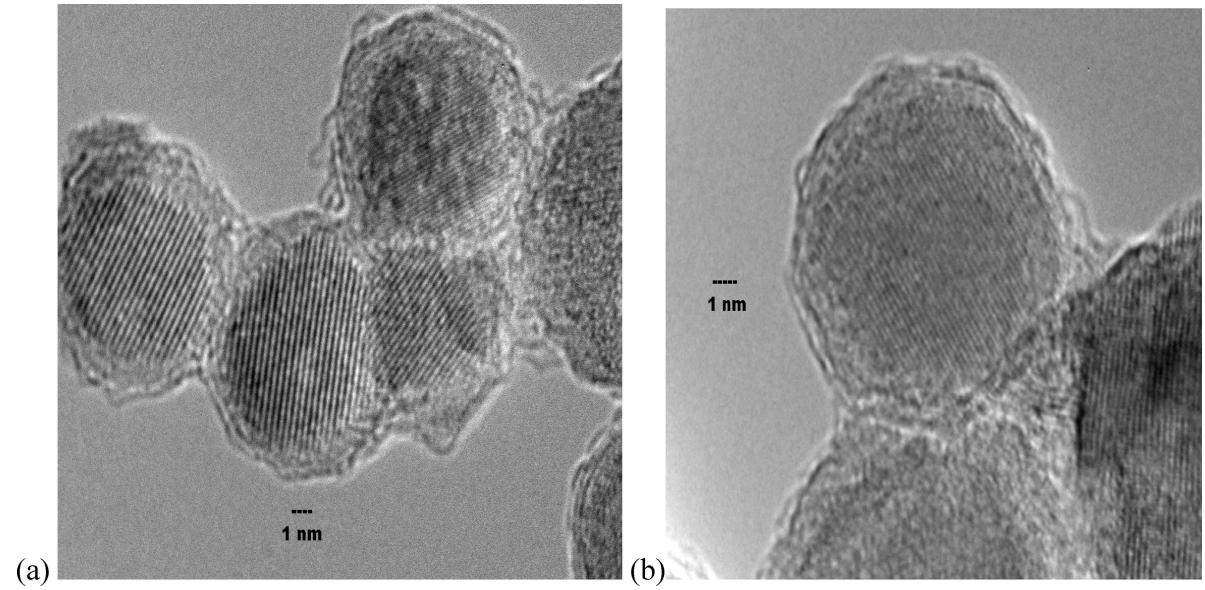

Figure 4. HR-TEM images of (a) 50 mol% CeO_x in Al_2O_3 (b) 75 mol% CeO_x in Al_2O_3.

nanopowders along the $CeO_x-Al_2O_3$ tie-line, their particle morphologies, phase compositions, surface chemistries, thermal properties.

Precursor and Precursor Formation. We previously reported the characterization of alumatrane [$N(CH_2CH_2O)_3Al$] and its use as a precursor in LF-FSP for the synthesis of δ-alumina nanopowders.[28] Here we report the synthesis and characterization of the precursor, $Ce(O_2CCH_2CH_3)_3(OH)$, as detailed in the experimental section. This precursor has a thermal decomposition pattern similar to other metal carboxylate precursors studied previously.[25–34]

Figure **1** shows a TGA trace for $Ce(O_2CCH_2CH_3)_3(OH)$. Initial mass losses (3%) are due to propionic acid of recrystallization and solvent. Thereafter, mass loss events are attributed to decomposition of the propionate ligands as suggested by reactions (1)–(3).

$$Ce(O_2CCH_2CH_3)_3(OH) \rightarrow Ce(O_2CCH_2CH_3)_2(OH)_2 + CH_3CH{=}C{=}O \quad (1)$$

Mass loss Calc (Found) = 14.45% (15%).

$$Ce(O_2CCH_2CH_3)_2(OH)_2 \rightarrow Ce(OH)_4 + 2[CH_3CH{=}C{=}O] \quad (2)$$

Mass loss Calc (Found) = 28.90% (29%).

$$Ce(OH)_4 \rightarrow CeO_2 + 2H_2O \quad (3)$$

Mass loss Calc (Found) = 9.28% (9%).

Final ceramic yields (44% CeO_2) are within experimental error of the calculated values (44.37%) for the decomposition of the precursor [$Ce(O_2CCH_2CH_3)_3(OH)$] to oxide (CeO_2) and are as expected on the basis of previous studies.[25–34]

Compositions of As-Processed Nanopowders. Fifteen different precursor compositions in the $(CeO_x)_x(Al_2O_3)_{1-x}$ system were prepared by making simple mixtures of alumatrane and the propionate as detailed in the Experimental. Compositions were confirmed by XRF. These nanopowders were analyzed by XRD, BET, HR-SEM, HR-TEM, STEM, XEDS, FT-IR, and TGA-DTA as discussed in the following sections.

XRD Powder Pattern Studies. Figure **2** provides XRD patterns for as-produced nanopowders along the $(CeO_x)_x$-$(Al_2O_3)_{1-x}$ tie-line. Samples with CeO_x concentrations $\leq$5 mol % show only the transition alumina phase (δ*-alumina) found for undoped LF-FSP powders.[28] As noted in a previous publication, at these concentrations, the cerium is present as Ce^{3+} and replaces Al^{3+} in the δ*-Al_2O_3 lattice as witnessed by its cathodoluminescence behavior.[19,20]

XRD patterns of samples with CeO_x concentrations between 5 and 10 mol % show the presence of both cubic CeO_2 (see below) and evidence that a considerable portion of the Ce^{3+} ions are present as Ce-magnetoplumbite ($CeAl_{11}O_{18}$).[19b] Ce−magnetoplumbite has a spinel structure separated by hexagonal planes containing Ce^{3+} ions.[39–41] δ*-Alumina or Ce−magnetoplumbite vary only by the number (1 or 3) of oxygen atoms in the rare earth plane, respectively.[39–41]

Powders with concentrations above 10 mol % ceria show only the cubic CeO_2 phase because of the relative high peak intensity of ceria XRD patterns over alumina. However, both cubic ceria and δ*-alumina co-exist as confirmed by TEM, XEDS, and XRF in the following sections.

Average Particle Sizes (APSs) and Specific Surface Areas (SSAs) from BET. The APSs for these materials were estimated from Debye−Scherrer line broadening and their SSAs (Table **1**). Both methods give similar results with the BET values tending to be somewhat bigger. In general, the average SSAs for the samples are 55 $\pm$ 10 m^2/g, giving APS values of 15 $\pm$ 5 nm.

Scanning Electron Microscopy (SEM) Studies. SEM was used to demonstrate powder uniformity. (Figure **3**) shows that SEM resolution is insufficient to reveal individual particles but does provide a view of the general particle population. These SEM images indicate that the particle populations produced here do not include any obvious micrometer-sized particles.

(41) Okada, K.; Hattori, A.; Taniguchi, T.; Nukui, A.; Das, R. N. *J. Am. Ceram. Soc.* **2000**, *83* (4), 928.

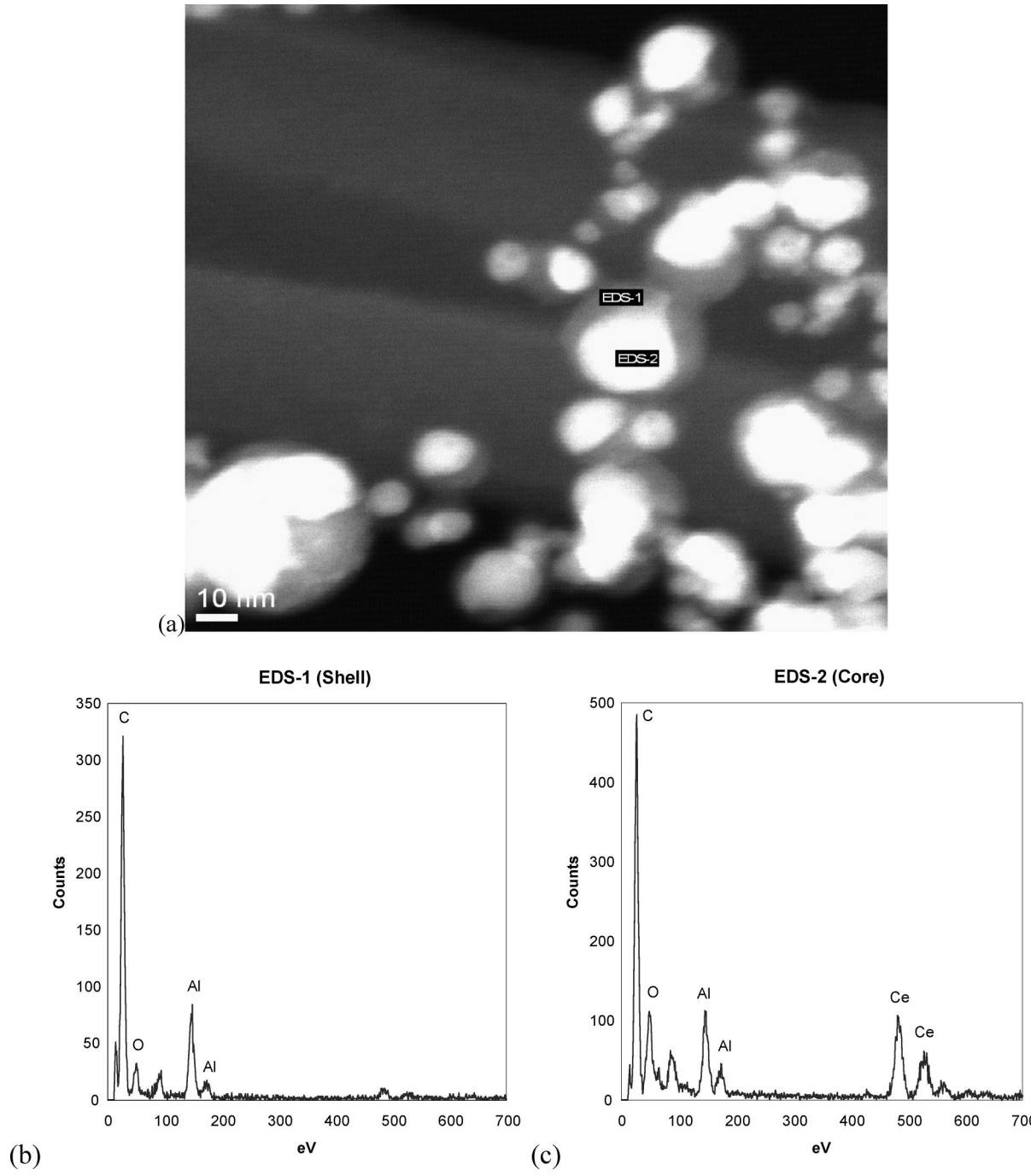

Figure 5. (a) STEM image and (b, c) XEDS of core−shell $(CeO_x)_{0.5}(Al_2O_3)_{0.5}$.

High-Resolution TEM (Transmission Electronic Microscopy) Studies. TEM images were used to gather information on particle morphologies and sizes of as-prepared powders. Discussions of actual size/size distributions are not appropriate if based solely on TEM micrographs, unless combined with the XRD results and SEM images. Figure **4** offers high-resolution TEM images of $(CeO_x)_x(Al_2O_3)_{1-x}$ nanopowders from LF-FSP. Particle sizes here are typically below 30 nm in diameter with the vast majority <20 nm.

In Figure **4**, clear lattice fringes in particle cores show a high degree of crystallinity of the CeO_x. Phase segregation between cubic ceria and δ*-alumina can be presumed from these core−shell TEM images. Because elements with high Z numbers are darker in HR TEM images, the ceria core and alumina shell can easily be distinguished. Although the particles appear to be highly necked (aggregated), they are easily dispersed through ultrasonication, with dispersions staying stable for up to 72 h without sedimentation.

Particle Formation Mechanism. At the lowest concentrations of CeO_x (less than 10 mol %), Ce^{3+} ions are located in δ*-alumina lattice or Ce-Magnetoplumbite ($CeAl_{11}O_{18}$) as discussed above.[39–41] At higher ceria concentrations (≥30 mol % ceria), CeO_xparticles become encapsulated in Al_2O_3. We believe this is due to different nucleation and condensation processes.

During particle formation in the flame, species with lower vapor pressures can be expected to nucleate and grow earlier

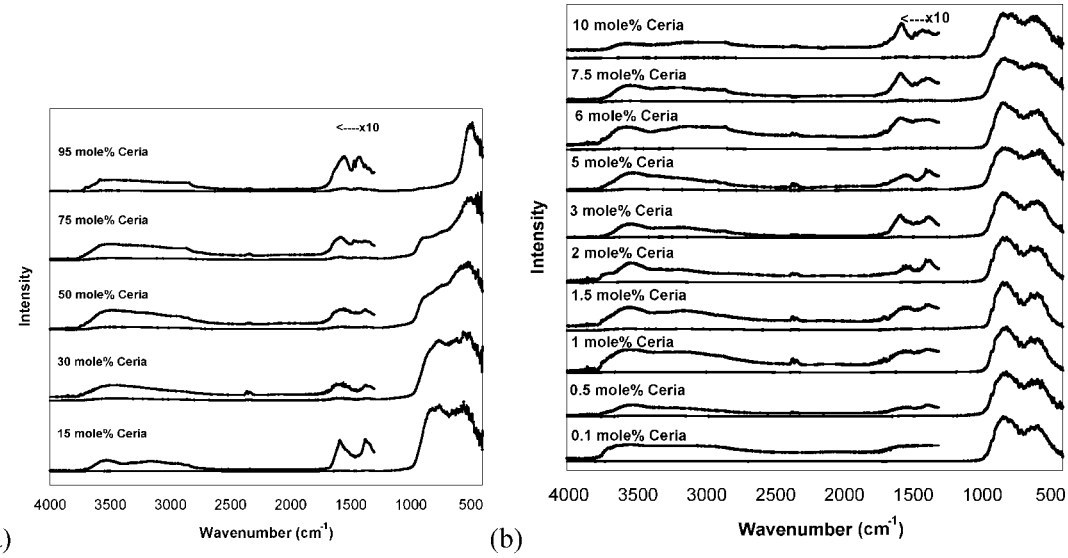

Figure 6. FTIR spectra of (a) ceria-rich and (b) alumina-rich $(CeO_x)_x(Al_2O_3)_{1-x}$.

at faster rates than species with higher vapor pressures. Given that Al_2O_3 has a lower vaporization temperature (3000 °C) than CeO_2 (3906 °C),[42,43] it seems reasonable to suggest that during the LF-FSP process, CeO_x species will nucleate and condense first followed by Al_2O_3. This results in homogeneous core−shell nanostructured nanopowders.

Because LF-FSP processing enables rapid quenching in a single step, core−shell ceria−alumina mixed-metal oxide materials form at nanosize level different from conventionally processed ceria−alumina binary materials. Note that we have recently reported similar results for LF-FSP produced $(ZrO_2)_x(Al_2O_3)_{1-x}$ nanopowders.[32]

STEM/XEDS. To determine where the cerium ions reside in as-produced powders, the STEM image in Figure **5** was obtained for a $(CeO_x)_{0.5}(Al_2O_3)_{0.5}$ sample. The large Z contrast between the Ce and Al ions is demonstrated by the distinctly brighter high Z core and darker alumina shells [dark cores and bright shells in normal TEM image Figure **4**] as corroborated by the XEDS analyses for the shell (EDS-1) and core (EDS-2) regions.

FTIR Spectra. Once the particle morphologies were characterized by XRD and high-resolution microscopy, the particle surface chemistries were characterized using FTIR per Figure **6**. All of the materials exhibit weak νOH absorptions in the 3700−3000 cm^{-1} region, attributable to surface hydroxyls arising from both physi- and chemisorbed water.[44] No νCH bands in the 3000−2700 cm^{-1} region were observed on the nanopowder surfaces.

Peaks attributable to surface confined CO_2 (1450 cm^{-1}) and carbonates (1620 cm^{-1}) are observed in the 1800−1400 cm^{-1}region in accord with those seen by Liu et al. and in our previous studies of pure δ-Al_2O_3 nanopowders.[28,45]

The lower wavenumber region shows νM−O bands typical for δ-alumina including two νAl−O bands at 810 cm^{-1} (stretching vibrations of tetrahedrally coordinated Al−O) and 610 cm^{-1} (octahedral coordination).[46,47] The νCe−O band at 460 cm^{-1} is not easily seen because it appears at the edge of resolution of our instrument.[48,49]

TGA-DTA Studies. Figure **7** records the mass loss events for the $(CeO_x)_x(Al_2O_3)_{1-x}$ composition nanopowders. All as-processed powders exhibit 1−1.5 wt % mass-losses up to ~300 °C typical of LF-FSP produced nanopowders, that can be attributed to evolution of both physi- and chemisorbed water as seen in the FTIR Figure **6**.[44] Mass losses between 300 and 400 °C are due to elimination of carbonate species.

Perhaps the most interesting observations are those at higher temperatures that appear to be associated with mass gains in the TGA at ca. 1200 °C with corresponding exotherms seen in the DTA Figure **8**. The most reasonable explanation for these mass gains is oxidation of residual Ce^{3+}. The solubility of Ce^{3+} in δ-Al_2O_3 is ≤5 mol %. $Ce^{3+/4+}$ are essentially insoluble in α-alumina.[50–52] Thus, we presume that the Ce^{3+} ions present in the δ-Al_2O_3 lattice or as magnetoplumbite segregate out during the δ to α alumina transformation and oxidize to CeO_2.

In Table **2**, we estimate the possible maximum amounts of Ce^{3+} ions from the mass gains above the ceria solubility limit. The mass gain of each composition is assumed to be oxygen as Ce^{3+} ions oxidize to CeO_2. Given the amounts of magnetoplumbite seen in these samples, and as suggested by a reviewer, the TGA experiments may not "see" all of the Ce^{3+} species present. Thus, it was necessary to conduct XPS studies as discussed in the following section.

(42) Jossen, R.; Pratsinis, S. E.; Stark, W. J.; Madler, L. *J. Am. Ceram. Soc.* **2005**, *88* (6), 1388.
(43) *CRC Handbook of Chemistry and Physics*, 80th ed.; CRC Press: Boca Raton, FL, 1999.
(44) Peri, J. B. *J. Phys. Chem.* **1965**, *69*, 211.
(45) Liu, X.; Truitt, R. E. *J. Am. Chem. Soc.* **1997**, *119*, 9856.
(46) Saniger, J. M. *Mater. Lett.* **1995**, *22*, 109.
(47) Tarte, P. *Spectrochim. Acta* **1967**, *23A*, 2127.
(48) Bouchara, A.; Rozes, L.; Soler-Illia, G. J.; DE, A.A.; Sanchez, C. *J. Sol−Gel Sci. Technol.* **2003**, *26*, 629.
(49) Harrison, P. G.; Daniell, W. *Chem. Mater.* **2001**, *13*, 1708.
(50) Dewing, E. W.; Haarberg, G. M.; Rolseth, S.; Ronne, L.; Thonstad, J.; Aalberg, N. *Metall. Mater. Trans. B* **1995**, *26B*, 81.
(51) Prakash, A. S.; Shivakumara, C.; Hegde, M. S. *Mater. Sci. Eng. B* **2007**, *139*, 55.
(52) Sasikala, R.; Sudarsan, V.; Kulshreshtha, S. K. *J. Solid State Chem.* **2002**, *169*, 113.

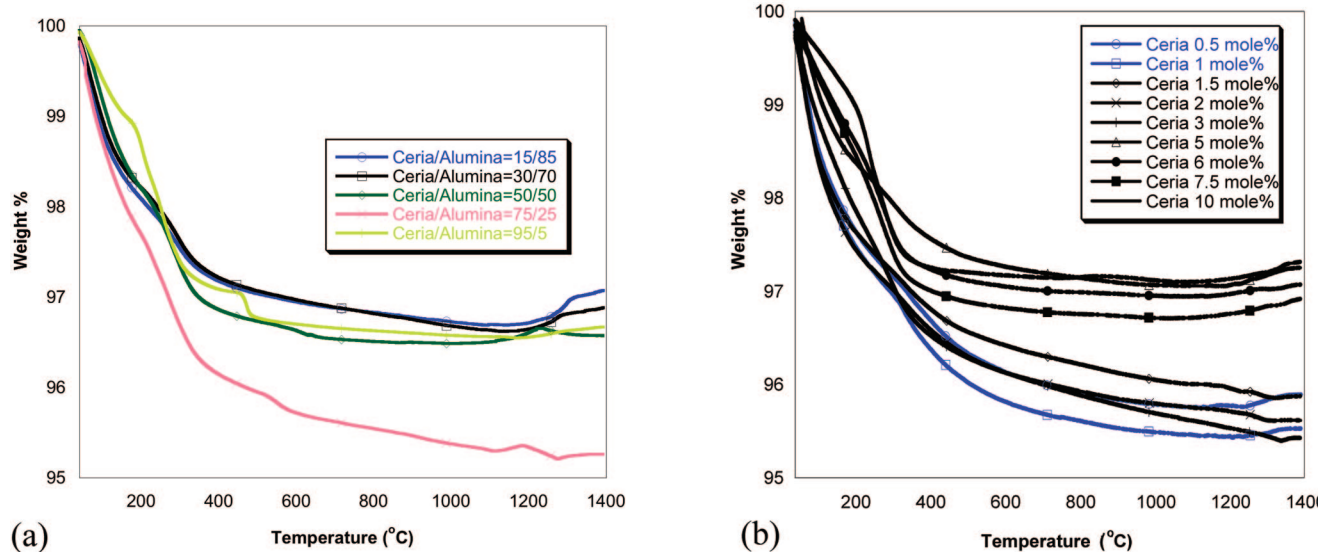

Figure 7. TGA of as-processed (a) ceria-rich and (b) alumina-rich $(CeO_x)_x(Al_2O_3)_{1-x}$ ramped at 10 °C/min in air.

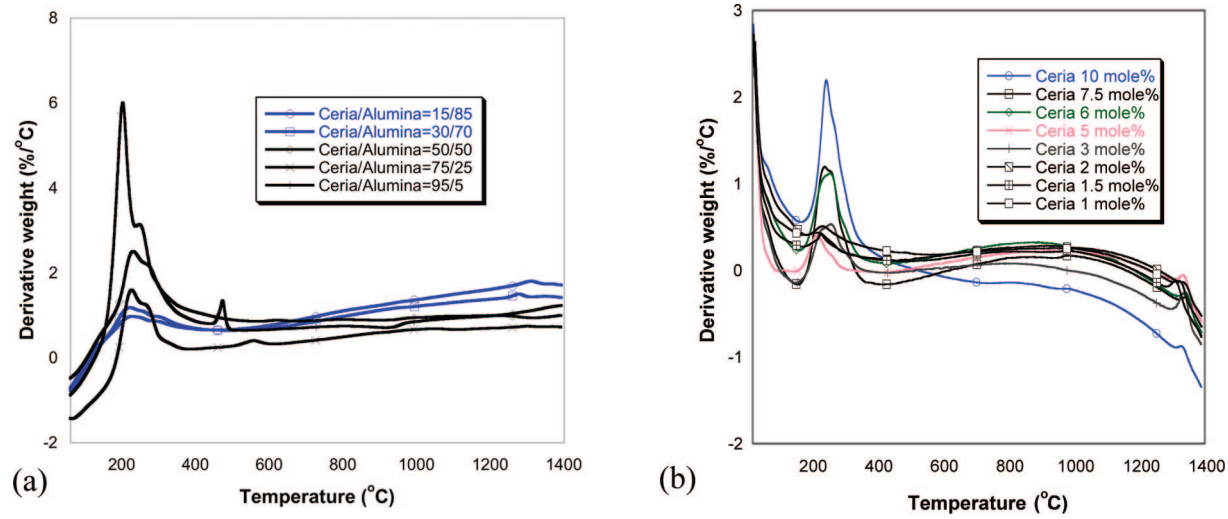

Figure 8. DTA of as-processed (a) ceria-rich and (b) alumina-rich $(CeO_x)_x(Al_2O_3)_{1-x}$ ramped at 10 °C/min in air.

Table 2. Possible Maximum Portions of Dissolved Ce^{3+} Ions in δ-Alumina

ceria mole %	mass gain (wt %)	possible maximum Ce^{3+}[a] (mol ± 0.1%)
30	0.30	0.7
15	0.32	0.7
10	0.21	0.4
7.5	0.20	0.4
6	0.18	0.3
5	0.15	0.3

[a] Assumes all reduced species are Ce^{3+}.

XPS Studies. XPS (see Experimental Section) was used to further quantify the Ce^{3+} ions in our nanopowders. The XPS data for the ceria-rich and alumina-rich samples Figure **9** indicate the presence of significant amounts of both Ce^{3+} and Ce^{4+} ions.[53,54] Relative $Ce^{3+/4+}$ ratios were obtained by quantification of XPS data (CasaXPS program) as presented in Table **3**.

XPS indicates that Ce^{3+} ions exist in both ceria- and alumina-rich samples. These results are unexpected and may relate to core−shell effects wherein the shell prevents oxidation of the Ce^{3+} to Ce^{4+} in the highly oxidizing environment of the flame. This may be the reason that these materials turn out to be quite good catalysts for a variety of oxidizing reactions and the water gas shift reaction, as we will report at a later date.[55] These results are important and deserve further study.

As with many of our previous studies, LF-FSP materials generated by rapid quenching lead to novel kinetic products not expected based on traditional processing methods that typically drive formation through thermodynamic assumption on particle mixtures. Because traditional processing methods lead to thermodynamically rather than kinetically defined phase compositions, these materials may offer unique opportunities for variety of applications.

(53) Zhu, H. Y.; Hirata, T. *J. Mater. Sci. Lett.* **1993**, *12*, 749–751.
(54) Gigola, C. E.; Moreno, M. S.; Costilla, I.; Sanchez, M. D. *Appl. Surf. Sci.* **2007**, *254*, 325–329.
(55) Maier,W. ; Kim,M. ;Laine, R.M. unpublished results.

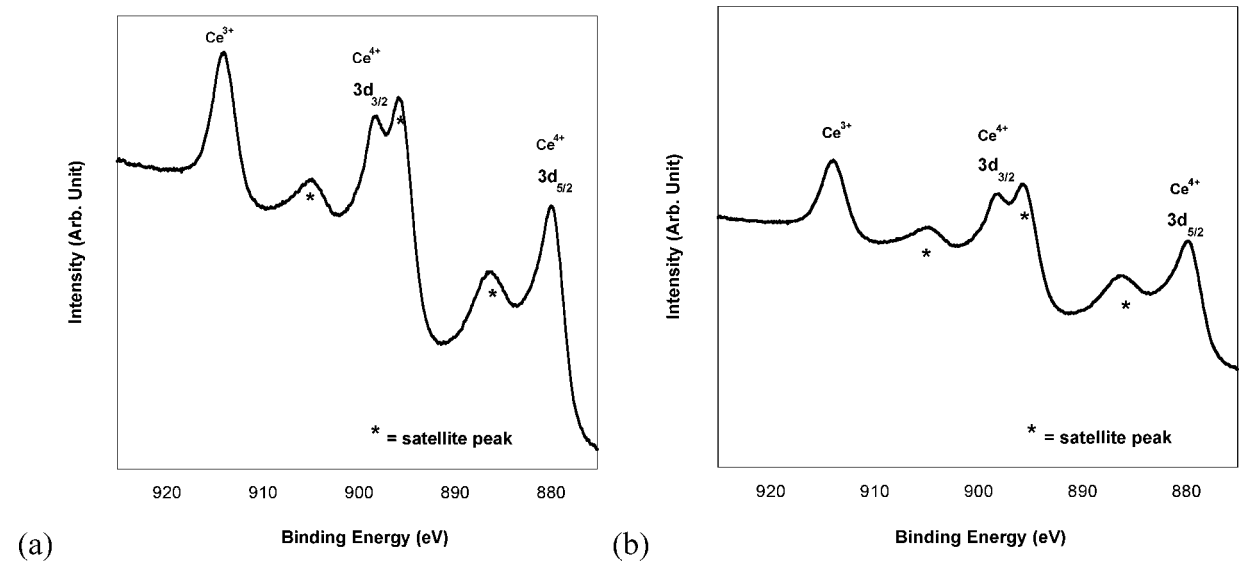

Figure 9. XPS of (a) 6 mol % CeO_x in Al_2O_3 and (b) 75 mol % CeO_x in Al_2O_3.

Table 3. Quantification of $(CeO_x)_x(Al_2O_3)_{1-x}$ XPS data

sample	Ce^{3+}/Ce^{4+} ratio
6 mol % CeO_x	0.17
75 mol % CeO_x in Al_2O_3	0.19

From our previous study, Ce^{3+} in Al_2O_3 can also offer potential for photonic applications such as sensor, laser and display materials.[22–24]

Conclusions

LF-FSP provides access to $(CeO_x)_x(Al_2O_3)_{1-x}$ mixed-metal oxide nanopowders with exceptional control of stoichiometry and phase purity. We were able to produce nanopowders of any composition in the $(CeO_x)_x(Al_2O_3)_{1-x}$ phase field with specific surface area of ≥ 50 m^2/g at rates of 100−300 g/h. Most of all, we succeeded in preparing core−shell nanoparticles in the $(CeO_x)_x(Al_2O_3)_{1-x}$ system in a single step, at CeO_x rich compositions (≥ 15 mol%). We also found the presence of Ce^{3+} ions in δ-alumina lattice at all concentrations and Ce−magnetoplumbite at 5−10 mol % CeO_x concentrations.

Because LF-FSP offers rapid quenching of the combustion species, it provides access to new, kinetic materials not accessible by any other conventional processing method. Thus, we find the presence of Ce^{3+} ions in nanopowders of Ce−Al−O system, Ce−magnetoplumbite structure and $(CeO_x)_x(Al_2O_3)_{1-x}$ core−shell nanostructured nanoparticles at specific CeO_x compositions. These nanopowders can offer novel potential for catalytic, structural, photonic, and electronic applications.

Acknowledgment. We thank the Air Force Office of Scientific Research for support of this work through Contract No. F49620-03-1-0389.

CM703382X